CONIN H2020-MSCA-RISE-2016

Action acronym: CONIN

Action full title: Effects of confinement on inhomogeneous systems

Grant agreement No 734276

Work Package 2

Modelling of systems with dominant electrostatic interactions (Months: 1-48)

Task 2.2

Development of the theory of phase transitions in ionic liquids

(Months: 13-24)

Deliverable D2.2

Structural properties and phase diagrams of ionic liquids in disordered porous media

In 2018 the planned task was:

Task 2.2: **Development of the theory of phase transitions in ionic liquids**

"Using the method of CVs in combination with the methods of the theory of associative liquids, we will further develop the theoretical approach for the study of vapour-liquid and liquid-liquid phase transitions in ionic liquids. Several models of ionic liquids with simple and complex structures will be considered with and without a solvent compound. The phase diagrams will be calculated and their dependence on the model parameters will be analysed. The obtained results will be compared with computer simulation data. Lead Participant: ICMP (O. Patsahan). ICMP, IPC, CPT, BSTU, CSIC will perform analytical, numerical and simulation studies."

In addition, the studies planed in Task 2.3 have been started.

Task 2.3: **The effects of confinement on the structure and diffusion properties of simple and complex ionic systems**

"We plan to study the effect of grain boundaries in ceramic solid electrolytes and intercalation compounds and electrode/electrolyte boundaries in solid and liquid electrolytes on the spatial distribution of charge carriers, ion diffusion and electric current. The microscopic models accounting of non-homogeneous character of the systems under consideration will be developed. The gradient contributions in the areas of large concentration gradients will be taken into account. Analytical findings will be compared with Monte Carlo simulation results and available experimental data."

The activities in WP2 in 2018 were the following:

1. **Development of the theory of phase transitions in ionic liquids**

   (a) Primitive models of room temperature ionic liquids. Liquid-vapour phase coexistence.

   (b) Phase behaviour in ionic solutions: restricted primitive model of ionic liquid in explicit neutral solvent of spherical molecules.

   (c) Phase behaviour in ionic solutions : restricted primitive model of ionic liquid in explicit neutral solvent of non-spherical molecules.

   (d) Liquid-vapour critical parameters of model ionic liquids confined in disordered porous media.

2. **Effects of confinement on the structure and diffusion properties of simple and complex ionic systems**

   (a) Electrical double layers close to ionic liquid-solvent demixing.

   (b) Optimization of charge-discharge cycles in nanoporous supercapacitors.

   (c) The effect of the crystal field variation on the screening effects and electro-physical characteristics.

   (d) The effect of short-range interaction and correlation on the charge and electric field distribution in a model electrolyte.

   (e) Non-monotonic concentration distribution of charge carriers in solid electrolyte between flat electrodes.

   (f) Cluster expansion for the description of condensed state: crystalline cell approach.

   (g) Monte Carlo simulation of diffusion and electric conductivity in Coulomb systems.

1. Development of the theory of phase transitions in ionic liquids

1a. Primitive models of room temperature ionic liquids. Liquid-vapour phase coexistence

We proposed several versions of primitive models of room temperature ionic liquids (RTILs) and develop a mean spherical approximation (MSA)- type theory for their description. RTIL is modelled as a two-component mixture of hard-sphere anions and flexible linear chain cations, represented by tangentially bonded hard spheres with the charge located on one of the terminal beads. The general schematic representation of the considered models is presented in Fig. 1a. The theoretical description of the model is carried out using the

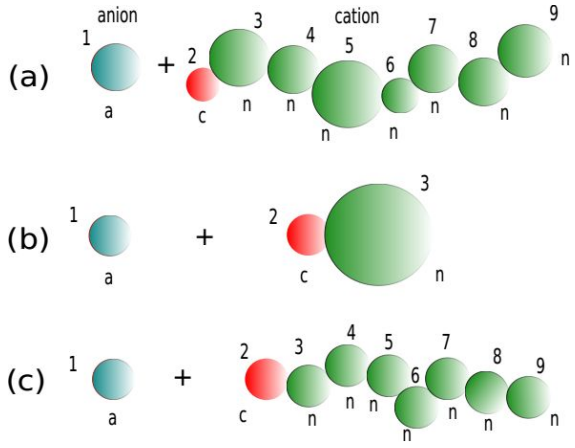

FIG. 1: Schematic representation of the primitive models of the RTIL. The general version of the model (a) and its dimer (b) and chain (c) versions, D and C, respectively.

solution of the appropriately modified associative MSA (AMSA) [1]. The problem reduces to solving one nonlinear algebraic equation for the Blum's screening parameter Γ, which, in turn, is used to express all thermodynamic properties of the models of interest [2]. We calculate liquid-vapour phase diagram using theoretical and computer simulation methods for two versions of the model, represented by the dimer (D) and chain (C) models presented in Fig. 1b and Fig. 1c correspondingly. The comparison of the liquid-vapour phase diagram for both types of model is presented in Figs. 2-3. As one can see, the theoretical predictions for the phase diagrams appear to be in reasonably good agreement with computer simulation results. Finally in Fig. 4 we compare our results for the critical temperature of the model C

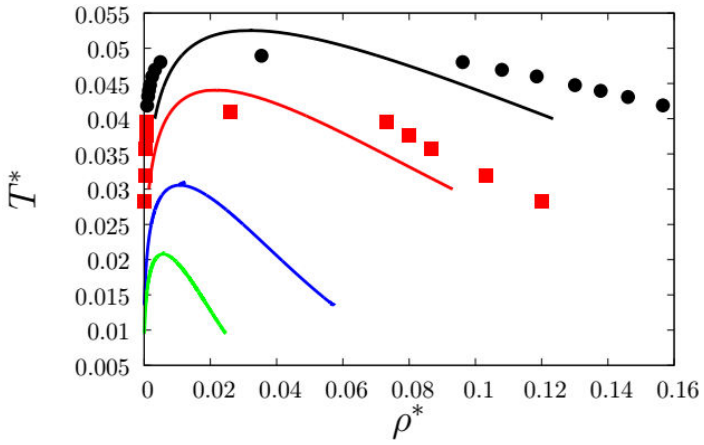

FIG. 2: Liquid-vapour phase diagram of model D, with the cation represented by the dimer ($m_c = 2$) with different hard-sphere sizes of the neutral bead, i.e. $\sigma_n = 0$, σ, 2σ, 3σ (from the top to the bottom) shown by the solid black, red, blue and green lines, respectively. Here $\sigma_c = \sigma_a = \sigma$. Black circles and red squares represent computer simulation results [3] for the models with $\sigma_n = 0$ and with $\sigma_n = \sigma$, respectively.

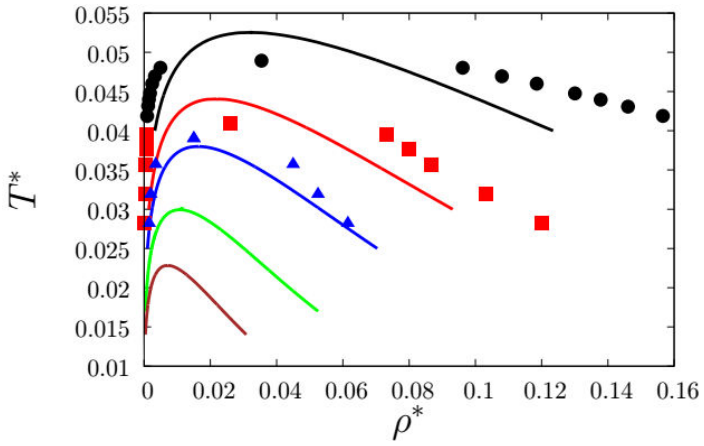

FIG. 3: Liquid-vapour phase diagram of model C, with equal hard-sphere sizes for all monomeric units ($\sigma_a = \sigma_c = \sigma_n = \sigma$) and different lengths of the cation chains $m_c = 1, 2, 3, 4, 5, 8$ (from the top to the bottom) shown by the solid black, red, blue, green and brown lines, respectively. Black circles, red squares and blue triangles represent computer simulation results [3] for the models with $m_c = 1$, $m_c = 2$ and $m_c = 3$, respectively

.

against the corresponding results obtained by extrapolating the experimental data for the

surface tension and density of a homologous series of imidazolium-based ionic liquids, i.e. [$C_n$mim][BF_4], [$C_n$mim][PF_6] and [$C_n$mim][Ntf_2] [4]. It is demonstrated that the models and the theory are able to qualitatively reproduce the experimentally observed phase behavior of RTILs, in particular, the decrease of the critical temperature and critical density with increasing asymmetry of the model in its shape and position of the charge. Further improvement of our results can be achieved by recognizing that the dielectric permittivity ϵ in the expression for the Coulomb potential can take different values. For imidazolium-based RTIL with ions lacking polar groups, the dielectric permittivity is related to refractive index n_D, i.e. $\epsilon = n_D^2$. The theory proposed appears to be in a very good agreement with the experiment assuming that $\epsilon \approx 1.60 - 1.67$ (see Fig. 4).

The results were discussed at II CONIN workshop and are published in Ref. [5].

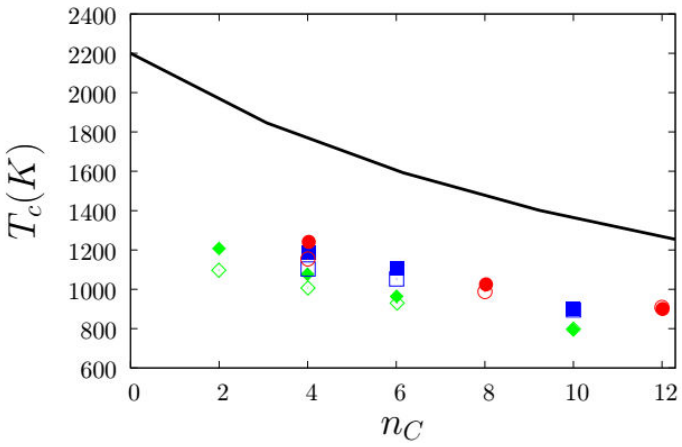

FIG. 4: Critical temperature $T_{cr}(K)$ as a function of the number of carbons in the imidazolium-based ionic liquids. Symbols denote experimental results for [$C_n$mim][BF_4] (red circles), [$C_n$mim][PF_6] (blue squares) and [$C_n$mim][Ntf_2] (green diamonds) and solid line denotes results of our theory. Here filled symbols represent results obtained using the Eötvos relation and open symbols denote results calculated using the Guggenheim relation

.

1b. Phase behaviour in ionic solutions: restricted primitive model of ionic liquid in explicit neutral solvent of spherical molecules

A comprehensive overview of the phase diagrams of ionic liquids (ILs) in a variety of polar and non-polar solvents and the comparison of these diagrams with the results of model systems, in particular, the primitive model (PM) and the restricted PM (RPM), show that more complex models should be used to properly describe these systems. In this connection, models that take the structure of solvents into consideration are of particular interest.

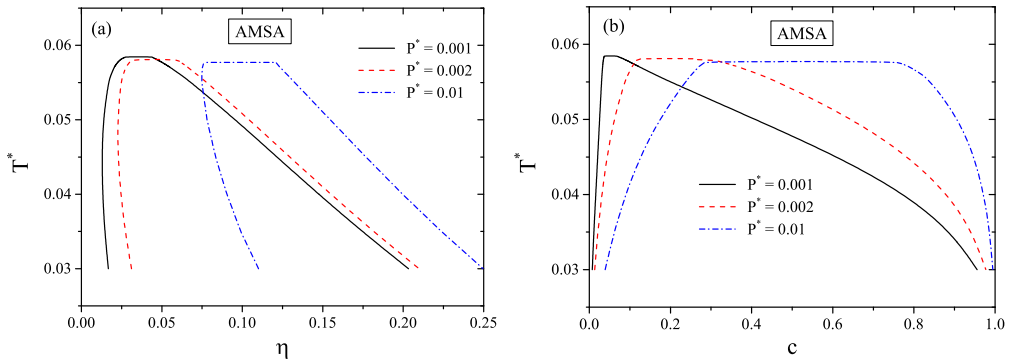

FIG. 5: Coexistence curves of the RPM-HS mixture presented in T^*-η (a) and T^*-c (b) planes at constant reduced pressures in the AMSA. The notations are as follows: $P^* = P\varepsilon\sigma^4/q^2$, $T^* = k_BT\varepsilon\sigma/q^2$, $\eta = \eta_i + \eta_s = \pi\rho\sigma^3/6$, $c = \rho_s/\rho$, where $\rho_{i(s)}$ is the number density of ions (solvent molecules), $q = q_+ = |q_-|$ is the ion charge, and σ is the hard-sphere diameter.

We have extended well-known theoretical approaches, i.e., the collective-variable-based (CV) theory, the mean-spherical approximation (MSA), and the associative MSA (AMSA) to the study of fluid-fluid phase equilibria in the model of ionic solutions that takes into account the presence of the solvent explicitly. Using the CV theory, we have found free energy, pressure and partial chemical potentials in the random phase approximation (RPA) for a rather general model that takes into consideration solvent-solvent and solvent-ion interactions beyond the hard core. In this work, we have focused on RPM-HS mixture consisting of oppositely charged hard spheres and neutral hard spheres. Within the RPA, we arrive at free energy in the Weeks-Chandler-Andersen (WCA) approximation by exploiting the WCA regularization of the Coulomb potential inside the hard core and at free energy in the ORPA/MSA by using the optimized regularization of the Coulomb potential. It should

be emphasized that the WCA approximation and the AMSA theory are applied to the study of the phase behaviour of the RPM-HS mixture for the first time. Despite the fact that the RPM-HS mixture had been previously studied by the MSA [8], in this paper we calculated the MSA phase diagrams for a wider region of thermodynamic parameters. Moreover, the calculation of the coexistence curves in the MSA serves as a verification of our results.

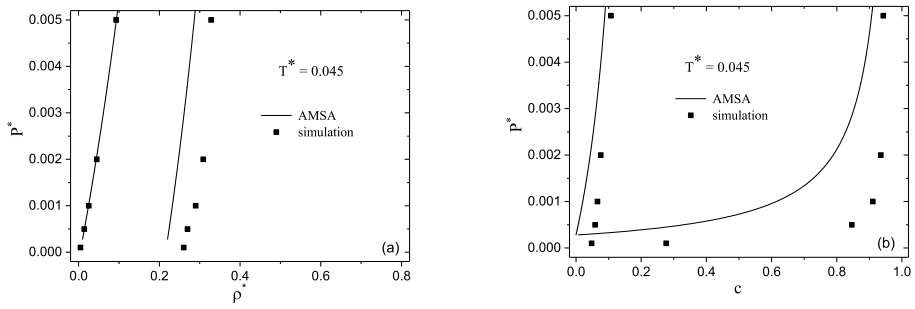

FIG. 6: Coexistence curves of the RPM-HS mixture presented in P^*-ρ^* (a) and P^*-c (b) planes at constant temperature $T^* = 0.045$. The lines are our AMSA results and the squares are the results of simulations [7]. $\rho^* = \rho\sigma^3$ and the rest of notations are the same as in Fig. 5.

We have calculated the fluid-fluid coexistence curves using the equations of phase equilibrium. The three above-mentioned approximations produce qualitatively similar results for the phase diagrams, i.e., an increase of pressure shifts a fluid-fluid coexistence region towards higher total number densities and towards higher solvent concentrations and at the same time leads only to a small increase of the critical temperature. It should be noted that the equations of the phase equilibrium yield more complex phase diagrams in the WCA approximation compared to the MSA and AMSA. In particular, they consist of upper and lower branches that form a closed loop with the lower critical solution point (LCSP). However, the thermodynamic analysis shows that a lower branch and the corresponding critical point are unstable. Remarkably, the LCSP and a nearly closed miscibility loop located in the metastable region were reported for an ionic solution in a non-polar solvent (the solution of $N_{4444}Br$ in toluene) [9]. A quantitative comparison of the results obtained in the three approximations indicates that critical temperatures provided by the AMSA are lower than in the WCA and MSA, while critical total number densities are higher. The phase diagrams calculated using the AMSA theory are presented in Fig. 5. As for a pure RPM,

the AMSA approximation leads to the best agreement with available simulation findings when the association constant proposed by Olaussen and Stell is used (see Fig. 6).

Discussions during the CONIN workshops helped to develop the theory. A final stage of the work have been done during the secondments of O.V. Patsahan and T.M. Patsahan from ICMP to BSTU. The results are published in Ref. [6].

1c. Phase behaviour in ionic solutions : restricted primitive model of ionic liquid in explicit neutral solvent of non-spherical molecules

We have developed the approach capable of describing the thermodynamics properties and phase transition behavior of binary mixture of ionic liquid and neutral solvent of non-spherical molecules. This approach is similar to that proposed for the case of solvent of spherical molecules and is based on the perturbation theory with a use of the associative mean-spherical approximation. The main problem of such a development is related with a correct description of the reference system, which in the present case consists of hard spheres and hard-core non-spherical particles. For this purpose, the scaled particle theory (SPT) is applied to describe the required reference system. In order to achieve the best fit with computer simulation results we have improved the SPT theory with a use the Carnahan-Starling-like and Parsons-Lee-like corrections and named this approximation as SPT2b-CS. As an example, the non-spherical particles were taken as hard spherocylinders (HSC) of length L_2 and diameter D_2, while hard spheres (HS) were taken of diameter D_1. Furthermore, we have also extended the SPT to the case of a binary HS/HSC mixture confined in a disordered hard sphere matrix (Fig. 7). It is worth noting that in HS/HSC mixtures when the length of HSC particles sufficiently large a nematic phase can appear. Therefore, orientation ordering can be observed at some densities. Moreover, the demixing processes occur in such systems and one can observe one phase (nematic) which is rich in HSC particles and another phases (isotropic) rich in HS particles. We have tested our theory for bulk and confined mixtures of HS/HSC particles. In Fig. 8a and Fig. 8b, we present some of our results where we compare our theoretical predictions with computer simulations.

We have shown that the SPT2b-CS approach is rather good in description of the thermodynamics properties of binary HS/HSC mixtures, including confined ones. Therefore, the SPT2b-CS can be used for the description of the reference system for the problem, where HS particles are charged and depict the restrictive primitive model (RPM) of ionic liquids in the

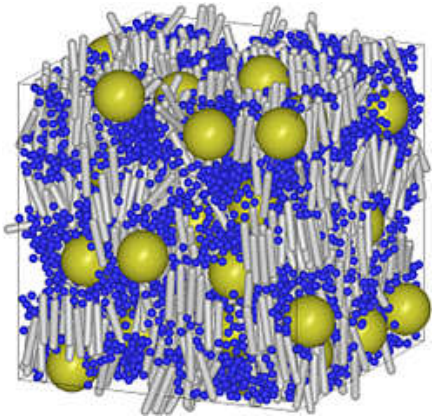

FIG. 7: Binary HS/HSC mixture in a HS matrix. Yellow particles denote matrix particles, blue and grey denote HS and HSC particles, respectively.

presence of neutral HSC solvent. We have already prepared a paper for publication where such a system is considered in the bulk, where the fluid-fluid phase transition in a RPM/HSC mixture have been studied. Now we are planning to investigate a confinement effect on this phase transition and also to clarify a role of orientation ordering of HSC solvent.

The work was started during the secondments of T. Patsahan and M. Hvozd from ICMP to BSTU. The results for a hard-core system were presented at the conference (oral presentation) [10] and are published in Ref. [11].

1d. Liquid-vapour critical parameters of model ionic liquids confined in disordered porous media

We have studied the vapour-liquid critical parameters of a charge- and size-asymmetric primitive model (PM) fluid in a disordered porous matrix composed of hard-sphere obstacles by using the collective-variables-based theory combined with an extension of the scale particle theory. The cations and the anions are characterized by point charges q_+ and q_- and by hard-sphere diameters σ_+ and σ_-, while the diameter of hard-sphere obstacles is σ_0. Our calculations are based on an explicit expression for the relevant chemical potential conjugate to the order parameter which takes into account the third order correlations between ions. In this paper, we have focused on the PM with $Z = q_+/|q_-| = 1$ and $Z = 2$. In the description of the results below, we use the following reduced units for the critical temperature and the critical density: $T_c^* = k_{\rm B}T_c\sigma_{+-}/(q_+|q_-|)$ and $\rho_c^* = \rho_c\sigma_{+-}^3$ where $\sigma_{+-} = \frac{1}{2}(\sigma_+ + \sigma_-)$.

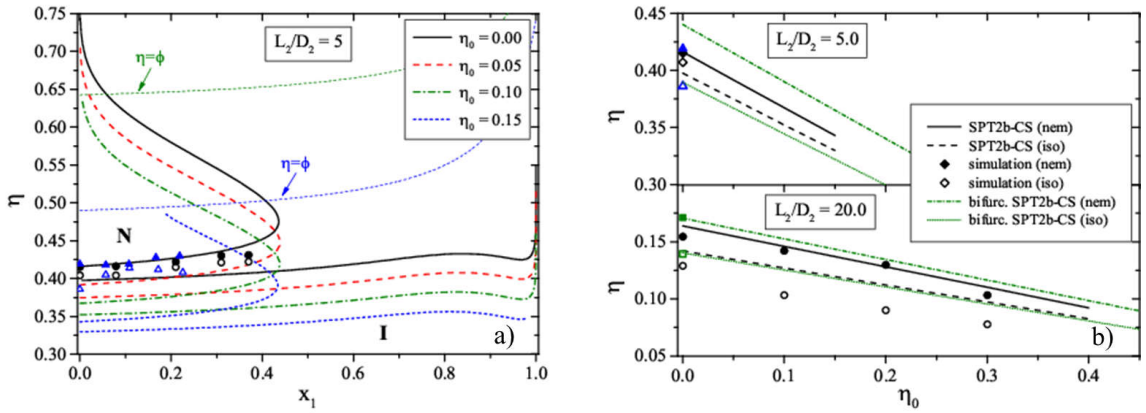

FIG. 8: (a) Isotropic-nematic coexistence diagrams obtained within the SPT2b-CS approach for the HSC/HS mixture with $L_2/D_2 = 5$ and $D_1 = D_2$ confined in matrices of different packing fractions $\eta_0 = 0.0 - 0.15$. Sizes of matrix particles equal to $D_0 = L_2$. Lines represent results obtained within the SPT2b-CS approach. The simulation results (symbols) taken from the literature are shown as circles and triangles, respectively. Dashed lines and open symbols correspond to highest densities of isotropic phase. Solid lines and solid symbols denote lowest densities of nematic phase. Thin dashed lines pointed by arrows with $\eta = \phi$ labels indicate boundaries at which the mixtures reach their maxima of packing fraction η in the corresponding matrices (green: $\eta_0 = 0.10$, blue: $\eta_0 = 0.15$). (b) Isotropic-nematic coexistence curves of a pure HSC fluid with $L_2/D_2 = 5$ (upper panel) and $L_2/D_2 = 20$ (lower panel) confined in matrices of different packing fractions $\eta_0 = 0.0 - 0.30$. Solid and dashed lines denote results obtained within the SPT2b-CS approach. Dash-dotted and dotted lines correspond to the results of bifurcation analysis. Simulation results taken from the literature are presented as symbols.

We have calculated the phase diagrams and the corresponding critical temperature T_c^* and the critical density ρ_c^* of 1:1 and 2:1 PM fluids at different values of size asymmetry ratios $\lambda = \sigma_+/\sigma_-$ and $\lambda_0 = \sigma_0/\sigma_-$ and at different values of matrix porosity ϕ_0. The results for the critical parameters are presented in Figs. 9 and 10. Our results have demonstrated the trends of the critical parameters which are common for the charge-symmetric and charge-asymmetric cases: (i) the critical temperature and the critical density are lower when the matrix porosity decreases; (ii) at a fixed porosity, both critical parameters are higher in a matrix of large particles than in a matrix of small particles; (iii) an increase in λ leads to the lowering of the critical temperature and the critical density. Despite these general

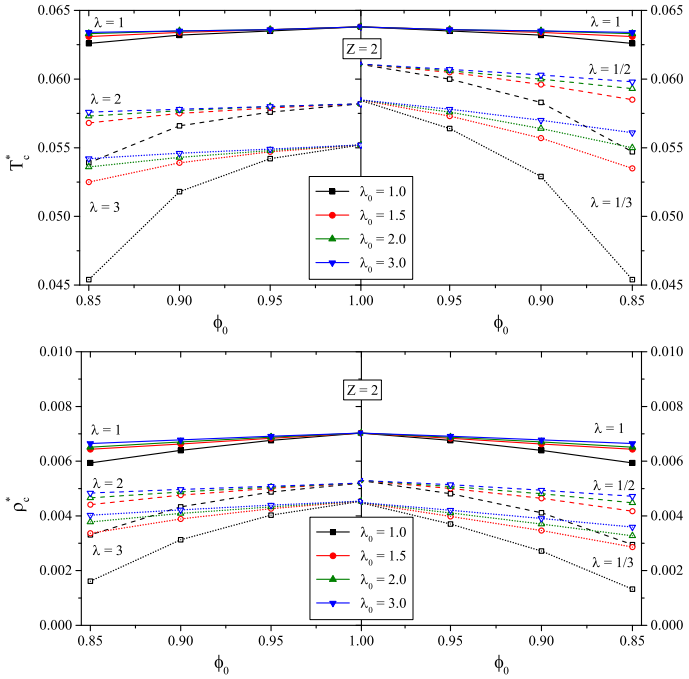

FIG. 9: Critical temperature T_c^* (upper figure) and critical density ρ_c^* (lower figure) of a confined PM fluid as a function of matrix porosity ϕ_0 for $Z = 2$. Solid lines correspond to the case of a PM fluid for $\lambda = 1$ (left and right panels), dashed lines – $\lambda = 2$ (left panels) and $\lambda = 1/2$ (right panels), dotted lines – $\lambda = 3$ (left panels) and $\lambda = 1/3$ (right panels). Symbols indicate which size of matrix particles λ_0 is used in each case.

trends we have found some peculiarities of the behaviour of the critical parameters of a confined charge-asymmetric ionic fluid. Our main conclusion is that for $Z = 2$ the effect of the matrix presence on the critical parameters is weaker when compared with the charge-symmetric case.

It is worth noting that our analytical theory gives a qualitative picture of the vapour-liquid phase behaviour of a charge- and size-asymmetric ionic fluid confined in a disordered porous medium. Nevertheless, the present study, to our best knowledge, is the first attempt to gain insight into this complicated problem.

The above results have been obtained in ICMP according to the plans described in the Grant Agreement. The results were presented at II CONIN workshop and are published in Refs. [12] and [13].

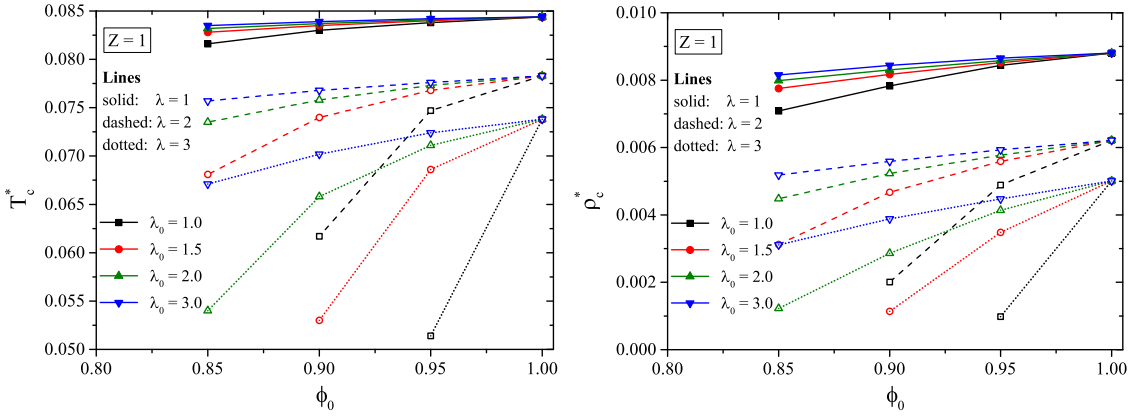

FIG. 10: Critical temperature T_c^* (left panel) and critical density ρ_c^* (right panel) of a confined PM fluid as a function of matrix porosity ϕ_0 for $Z = 1$. Solid lines correspond to the case of a PM fluid for $\lambda = 1$, dashed lines – $\lambda = 2$ and dotted lines – $\lambda = 3$. Symbols indicate which size of matrix particles λ_0 is used in each case.

2. Effects of confinement on the structure and diffusion properties of simple and complex ionic systems

2a. Electrical double layers close to ionic liquid-solvent demixing

Electrical double-layers (EDLs) play a key role in energy storage and have been suggested to have applications in energy generation. Recently, there has been an expansion of interest in EDLs, but EDLs with ionic liquid-solvent (ILS) mixtures received less attention. We have studied the temperature dependence of EDLs with ILS mixtures, in particular close to demixing. We postulated the grand potential of the form

$$\begin{aligned}\Omega[\rho_\pm, u]/A \;=\; & K\left[\int_0^\infty dz \frac{1}{2}\left(-\rho(z)^2 + \xi_0^2\left(\frac{d\rho(z)}{dz}\right)^2\right) + \frac{\xi_0}{2}\rho(0)^2 - h_0\rho(0)\right] \\ & + \int_0^\infty dz\Big[ec(z)\psi(z) - \frac{\epsilon}{8\pi}\left(\frac{d\psi(z)}{dz}\right)^2\Big] \\ & + k_BT\int_0^\infty dz\Big[\rho_+(z)\ln(a^3\rho_+(z)) + \rho_-(z)\ln(a^3\rho_-(z)) + \beta f_{ex}(\rho(z))\Big] \\ & - \mu\int_0^\infty dz\rho(z)\end{aligned} \tag{1}$$

where $\rho_\pm(z)$ is the number density of the cations and anions at distance z from an electrode, $\rho = \rho_+ + \rho_-$, $c = \rho_+ - \rho_-$, and μ is the chemical potential. The first line is a contribution

from attractive van der Waals interactions, where K and ξ_0 measure the strength and the range of the interactions, respectively; h_0 is selectivity (ionophilicity) of the electrode. The second line is the electrostatic energy, with e and ϵ being the elementary charge and the dielectric constant, respectively. The third line is an entropic contribution, with a being the ion diameter and $f_{ex}(\rho)$ the excess free energy associated with packing of the ions; we have taken $f_{ex}(\rho)$ in the Carnahan-Starling approximation.

Using the above model, we have demonstrated the emergence of a new type of the capacitance shape, in addition to the well-known camel and bell shapes, which manifests the fine interplay between the electrostatic and wetting properties of ILS mixtures. We find that the capacitance increases appreciably as the system approaches demixing, and this increase is accompanied by a sizable enhancement of the energy storage, which can be utilized for generating electricity from waste heat. The results are summarized in Figure 11.

The work has been performed at IPC (C. Cruz, A. Ciach and S. Kondrat) in collaboration with CSIC (E. Lomba). We discussed the problem with the members of other teams during the workshops and with visitors from BSTU seconded to IPC and CSIC. An article is submitted for publication.

2b. Optimization of Charge-Discharge Cycles in Nanoporous Supercapacitors

Nanoporous supercapacitors attract much attention as green energy storage devices with remarkable cyclability and high power and energy densities. However, their use in high frequency applications is limited by relatively slow charging processes. While the highest possible capacitance and energy densities are provided by ultra-narrow pores, such pores are known to show slow charge-discharge kinetics. We have studied the dynamics of charging nanoporous supercapacitors with such ultra-narrow pores by using molecular dynamics simulations. We revealed a transient formation of crowded and dilute ionic-liquid phases inside the pores, which leads to co-ion trapping and explains slow charging. However, we showed how trapping can be circumvented by applying a slow voltage sweep and we determined the *optimal* sweep rate, $k_{\rm opt}$, which minimize the charging times. Remarkably, this optimal rate behaves as $k_{\rm opt} \sim \ell^{-2}$, where ℓ is the pore length or electrode thickness. Conversely, the best *discharge* rates are obtained when the voltage is turned off in a step-like fashion, while the discharge times $\tau_{\rm dis} \sim \ell^2$. These 'scaling relations' allow one to predict optimal cycles for arbitrary thick electrodes. An example of such an optimal cycle for 8nm long pore is

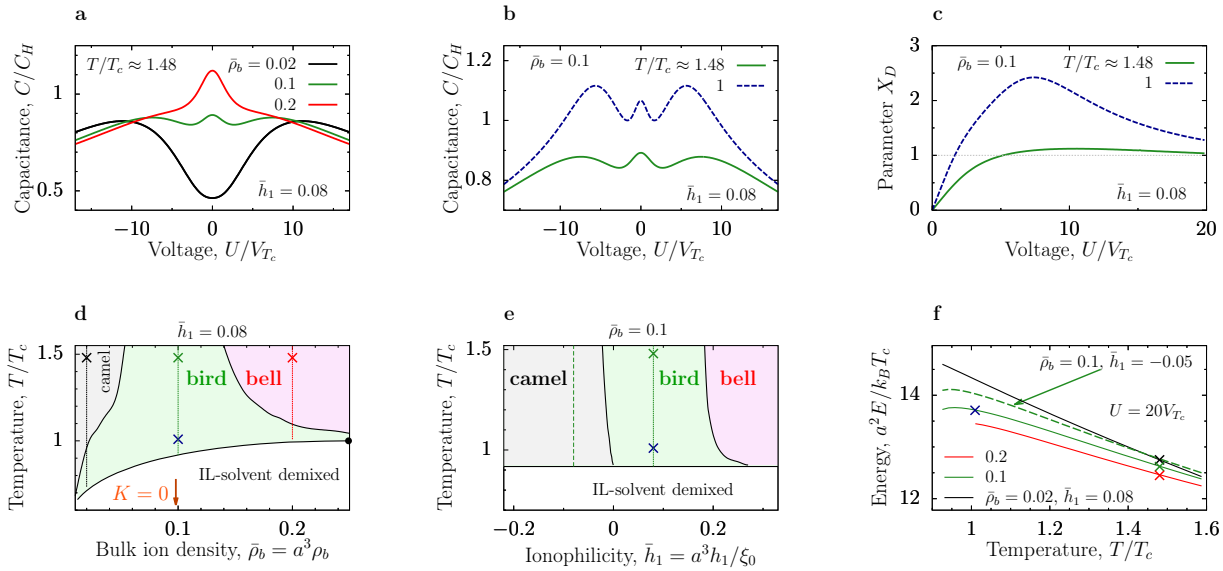

FIG. 11: Capacitance and energy storage close to demixing. (a) Differential capacitance C as a function of applied potential for constant temperature and various IL concentrations, demonstrating the camel, bird and bell-shaped capacitances. Voltage is measured in terms of thermal voltage $V_{T_c} = k_BT_c/e$ ($\approx$ 26mV at room temperature), and capacitance is measured in unit of $C_H = \varepsilon/4\pi a$ ($\approx 8\mu$F/cm^2 for $a = 0.7$nm with the permittivity of water at room temperature. (b) Effect of temperature on the bird-shaped capacitance. (c) Charging parameter $X_D = \Gamma/C$, where Γ is the adsorption of IL, as a function of voltage. (d) Capacitance diagram showing the regions with camel, bird and bell-like capacitances. The thin vertical lines denote the values of ρ used in (f) and the symbols show the values of the temperature and density used in (a-c). The arrow shows the location of the bell-to-camel transformation in the absence of dispersion forces ($K = 0$ in eq 1). (e) Capacitance diagram in the plane of temperature and electrode's ionophilicity (surface field $\bar{h}_1 = a^3h_1/\xi_0$). (f) Stored energy per surface area as a function of temperature for various IL concentrations and surface fields at an applied potential of $U = 20V_{T_c}$. Energy density is measured in units of $E_T = k_BT/a^2$ (≈ 0.84 μJ/cm^2 ≈ 0.23 nW·h/cm^2 for $a = 0.7$nm at room temperature).

shown in Figure 12. Interestingly, the optimal charge-discharge times are strikingly different, *viz.*, discharging is more than four times faster than charging. This time asymmetry has interesting implications, in particular that two Ragone plots are needed to describe fully the energy-power relation for supercapacitors, *viz.*, one for charging and one for discharging.

A part of this work was done by Svyatoslav Kondrat (IPC employee) during his second-

ment to BSTU, where discussions with V. Vikhrenko were particularly helpful. Questions concerning this work were discussed during the II CONIN workshop with the members of the other teams and invited lecturers, in particular with A. Kornyshev. The results are published in Ref. [14].

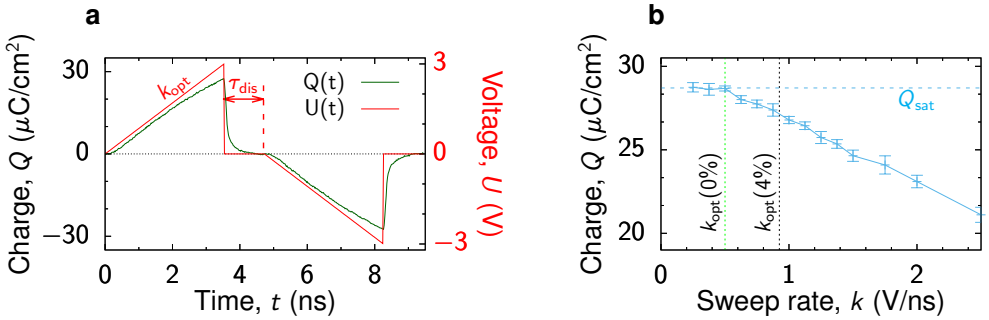

FIG. 12: Optimal charge-discharge cycle and sweep rate. (a) The full cycle consists of a linear sweep charging with the rate $k_{\rm opt}$ (panel b), followed by switching off the voltage in a step-like fashion. The next cycle begins in $\tau_{\rm dis}$ and can be either to positive or negative potentials. (b) Accumulated charge as a function of sweep rate. The optimal sweep rate with zero tolerance for undercharging permits charging to the maximal charge storage capability; charging times can be decreased but at the cost of a slight undercharging. The results show an average over 20 simulations.

2c. The effect of the crystal field variation on the screening effects and electro-physical characteristics

The lattice fluid model of the system with short-range and long-range Coulomb interactions is suggested. In the framework of the collective variables method, the screening of the Coulomb interactions in the bulk is considered and it is shown that the Debye length r_D includes additional concentration dependence inversely proportional to the square root of the mean concentration of vacant sites. Additionally, the contribution of the thermal ion displacements from the lattice sites to the Fourier transform of the screened Coulomb interaction is estimated. This contribution results in a more complicated wave vector dependence of the screened Coulomb interaction.

The Coulomb interaction contribution to the free energy of the system is calculated in the approach close to the mean spherical approximation and is given in an analytical form. The analysis of the concentration dependence of the chemical potential indicates (Fig. 13)

that the homogeneous distribution of mobile charges becomes unstable already at rather low concentration of particles where the concentration derivative of the chemical potential becomes negative. The region of the system stability can be determined more accurately due to consistent accounting of the short-range interactions and correlations among the mobile ions and especially with the particles of the neutralizing background.

In the mean field approximation, the mobile ions near the system boundary obey the Fermi-Dirac type distribution. When the interparticle correlations are taken into account, this distribution reminds the differential analog of the integral equation for the concentration distribution. The influence of the variation of the crystal field near the system boundary on the structure and characteristics of the electric double layer is investigated. As compared to the system with equal crystal potentials at the lattice sites throughout the system, the pronounced difference for the electric capacitance appears at low absolute values of the surface potential. For positively charged particles, this difference is more pronounced for negative electric potentials (Fig. 14).

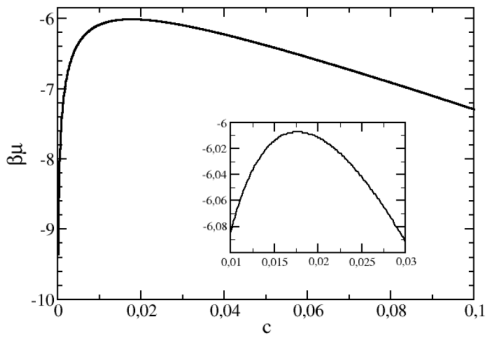

FIG. 13: The chemical potential versus concentration at $\epsilon = 40$, $T = 1000$ K, $b = 0.4$ nm, $d = 0.35$ nm, $r_D = 1.1$ nm, $r_B = 0.42$ nm.

The capacitance diverges at the potential values at which the electric field tends to zero and attains negative values in the regions of the surface potentials depending on their polarity and on the values of the surface crystal potential. From a mathematical point of view, the capacitance diverges at values of the surface potential at which the electric field tends to zero while the derivative of the square of the electric field over the electric potential is not equal to zero. From a physical point of view, the negative values of the capacitance and the system instability are due to the competition of the external electric field and internal crystalline

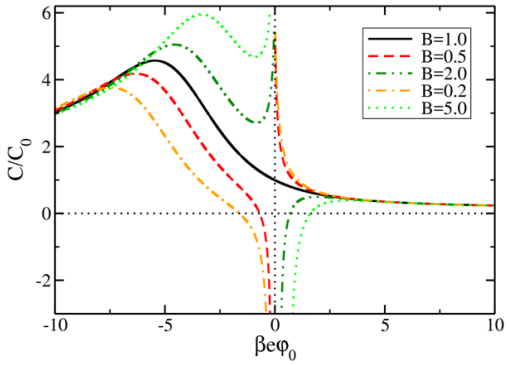

FIG. 14: The differential electric capacity C versus electric potential for positively charged particles. $C_0 = \epsilon/r_D$, $B = \exp(\beta\delta u)$, ϵ=40, $T = 1000$ K, $b = 0.4$ nm, $c = 0.01$, $r_D = 1.1$ nm.

field. Negative values of the capacitance may indicate the thermodynamic instability of the system although a more consistent taking into account of the short-range interaction contribution can considerably change the behavior of the system at low absolute values of the surface potential. In the description of the results below, we use the following notations: r_D is the Debye length, r_B the Bjerrum length, ϵ the dielectric constant, b the lattice spacing, d the hard core diameter of the particles, c the lattice concentration, β the inverse temperature, δu the variation of the crystal potential near the system boundary, φ_0 the surface electric potential. Black solid line in Fig. 14 corresponds to the system with uniform crystal field.

The work was performed during the secondments of the BSTU employees, Prof. Vyacheslav Vikhrenko and Dr. George Bokun (to CPT), the CPT employee Dr. Dung di Caprio and the ICMP employee Prof. Myroslav Holovko (to BSTU). The results are published in Ref. [15].

2d. The effect of short-range interaction and correlation on the charge and electric field distribution in a model electrolyte

A simple lattice model of a solid electrolyte presented as a xy-slab geometry system of mobile cations on a background of energetic landscape of the host system and in a compensating field of uniformly distributed anions, which are fixed at their positions is considered. The system is confined in the z-direction between two oppositely charged walls parallel to xy-plane. The combination of the mean field approach for the long-range part of Coulomb interaction and accounting of short-range cation-cation interactions and correlations for the inhomogeneous

systems is suggested to study the density distribution profiles of cations without and with an external electric field applied. Using the free energy minimization at each of z-coordinates, the corresponding set of non-linear equations for the chemical potential is derived. The set of equations was solved numerically with respect to the charge density distribution in order to calculate the charge distribution profile and the electrostatic potential in the system along z-direction under different conditions.

At a strong external electric field (high charge density at the confining walls c_w) a wide depleting zone near the positively charged wall is observed, which narrows with growing the average mobile charge concentration c (Fig. 15 and Fig. 16). The charge accumulates near the negatively charged wall where the short-range interactions result in a nonmonotonic charge distribution that are not seen in the mean field approximation. The depletion layer appears because of the electroneutrality condition. The lower is the cation concentration the larger volume of the system is required to fulfill this condition.

The effect of correlations is minor at the left wall due to the low cation concentrations and it is more pronounced at the right wall. The correlations lead to nonmonotonous charge distribution that is not observed in the mean field approximation. Moreover, the charge correlations lead to the deviation of the charge density from the average value near the walls even when the walls are not charged. These features become more pronounced at the larger average density $c = 0.1$, when the width of the near-wall structures decreases because of easier fulfilling the electro-neutrality condition and due to the smaller Debye length.

For the system of cations with the short-range attraction one can observe qualitatively different concentration profiles depending on the approximation applied. It is seen in Fig. 17a that for the case of average concentration $c = 0.03$ and uncharged walls the contact value of cations profile at the both walls is negative within the mean field approximation, while taking into account correlations results in the positive contact value. The same is observed for the larger average concentration $c = 0.10$. However, due to correlation effects the oscillating profile with periodic structure appears along z-direction (Fig. 17b) that is similar to what was found in systems with competing interactions. This result is expected, since in the model in fact the competing interaction between cations is introduced through the short-range attraction and the electrostatic repulsion on longer distances.

The work was performed during the secondments of the BSTU employees, Prof. Vyacheslav Vikhrenko and Dr. George Bokun (to CPT), the CPT employee Dr. Dung di Caprio

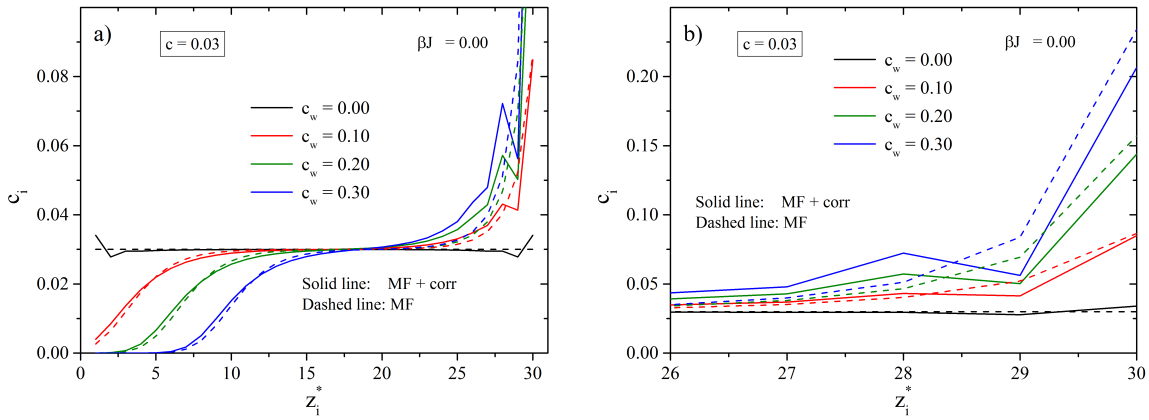

FIG. 15: Density profiles at low mean mobile charge density ($c = 0.03$). The concentration profile of cations between the walls of different charges ($c_w = 0.0 - 0.3$) and at the lower average concentration ($c = 0.03$). The dashed lines correspond to the results obtained within the mean field (MF) approximation and solid lines obtained with taking into account correlations (MF+corr). On the right panel, the region near the right wall is shown in a larger scale.

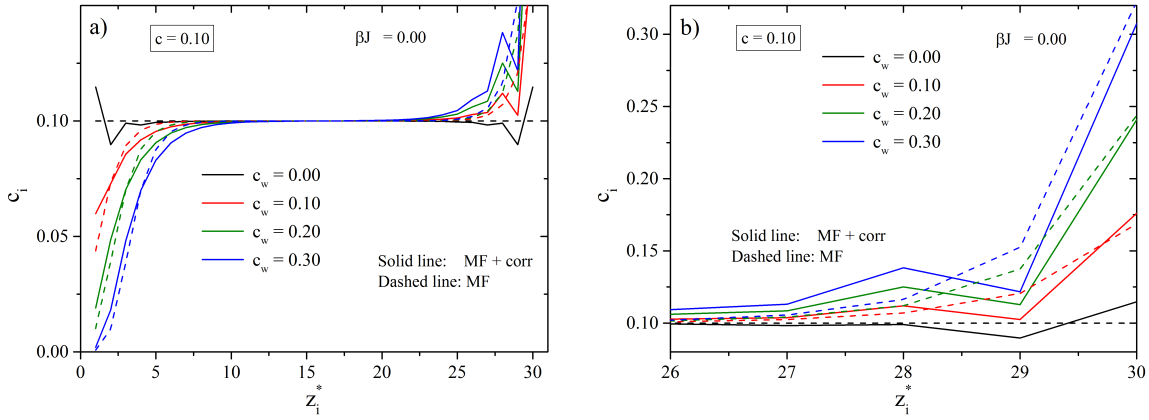

FIG. 16: The same as in Fig. 15, but at the higher average concentration of cations ($c = 0.10$).

and the ICMP employees Prof. Myroslav Holovko and Dr. Taras Patsahan (to BSTU). The results are presented at the conference and submitted to Solid State Ionic. The work is in progress and the collaboration will continue.

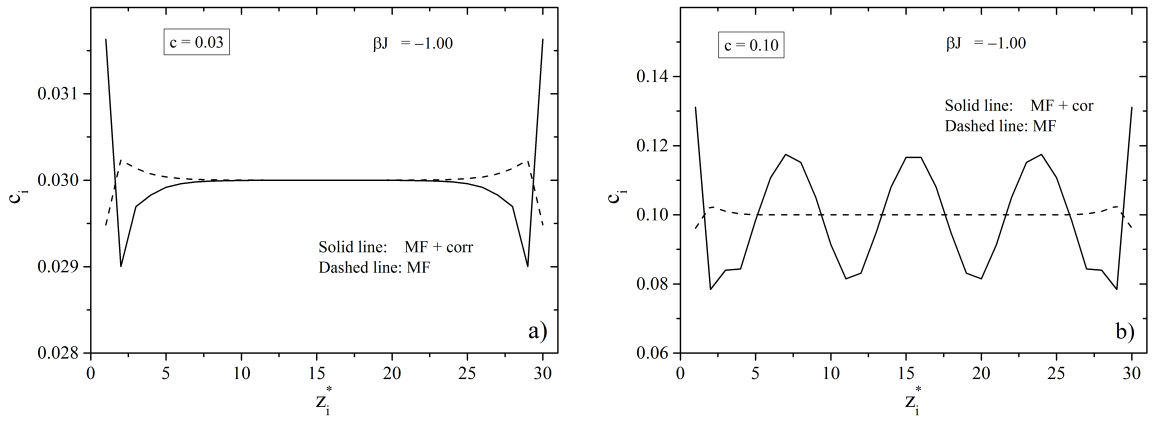

FIG. 17: The concentration profile of cations between uncharged walls ($c_w = 0.0$), but with taking into account the short-range attraction ($\beta J = 1.0$) at the low (left panel, $c = 0.03$) and high (right panel, $c = 0.10$) average concentrations. Comparison between the MF (dashed line) and MF+corr (solid line) approximations.

2e. Non-monotonic concentration distribution of charge carriers in solid electrolyte between flat electrodes

Mobile charges of one sort are considered in an external electric field in the presence of a compensating background of fixed charges of the opposite sign. The cell potentials of the method of conditional distributions are used to renormalize the Mayer functions. The cumulant expansion with respect to renormalized Mayer functions is used to represent the free energy of the subsystem of mobile charges in the form of a functional of their density distribution. The results of the method of collective variables (CVs) are used for the taking into account of the electric screening effects. A system of integral equations for the potentials of mean forces is obtained that accounts for the effects of short- and long-range interactions. The particular calculations are made in the lattice approximation. In the expression for the binary distribution function, the correlation component is extracted. The Poisson equation is used for calculating the correlated and uncorrelated parts of the electric potential. In the case of sufficiently small electric fields, a linear expansion of the chemical potential over the deviation of the charge concentration from the homogeneous distribution is considered. The correlation between particles is taken into account for the first neighbours. In this approximation, the distribution of potential and charge concentration is described by a linear differential equation of the fourth order. The analysis of its analytical solution and

the subsequent numerical calculations of the characteristics of solid electrolyte are performed.

It is shown that the electric field distribution obeys the expression

$$\psi = \frac{E\left((e^{k_1 x} - e^{-k_1 x}) - (2k_1/k_2)\sin(k_2 x)\right)}{2k_1\left((e^{k_1 L} + e^{-k_1 L}) - 2\cos(k_2 L)\right)},$$

where the origin of the coordinate system is chosen in the middle of the distance L between the electrodes, x and L are taken in units of the lattice spacing h, the electrode electric field E in $(\beta e^2/\epsilon\epsilon_0 h^2)$, e the electric charge, ϵ and ϵ_0 the dielectric and electric constants, consecutively, $\beta = k_B T$, k_B the Boltzmann constant, T the absolute temperature, k_1 and k_2 the imaginary and real wave numbers, respectively, in units of h^{-1}.

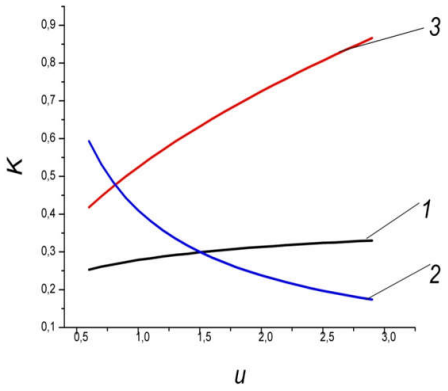

FIG. 18: The wave numbers versus $u = \beta e^2/(\epsilon\epsilon_0 h)$ at $s_h = 2$ and $c = 0.5$. 1 – k_1; 2 – $k = k_2 - 2.5$; 3 – k_D.

This electric field distribution results in the harmonic component imposed over the exponentially decaying charge distribution in the near electrode regions. The wave numbers depend on the following quantities: the ratio $s_h = J/(e^2/\epsilon\epsilon_0 h)$ of the short-range interaction energy J between the particles on the nearest neighbor lattice sites and the electrostatic energy for the same distance, the intensity of interparticle correlations, and the thermodynamic conditions (the particle lattice concentration c and temperature T). $k_1 = k_D$ and $k_2 = 0$, where k_D is the inverse Debye length, if the short-range interactions and correlations are neglected.

The dependence of the wave numbers on the inverse temperature is presented in Fig. 18. It follows from the figure that the short-range interactions strongly enlarge the near electrode exponentially decaying region (k_1 two to three times smaller of k_D). The distribution of the electric field and the concentration deviations are shown in Fig. 19.

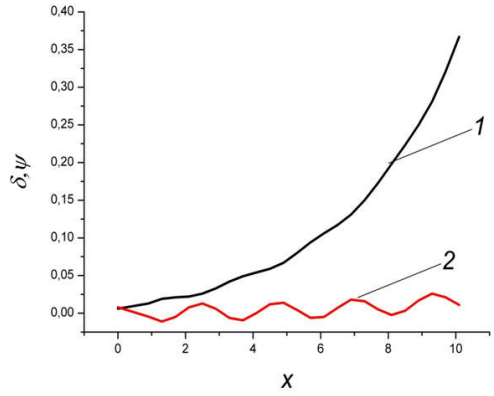

FIG. 19: The dimensionless electric potential ψ (curve 1) and concentration deviation of the charge carriers δ (curve 2) at $s_h = 2$ and $c = 0.5$. The electrode is disposed at $x = 10$.

The work was performed during the secondments of the BSTU employee, Dr. George Bokun (to CPT) and the CPT employee Dr. Dung di Caprio (to BSTU). The results are submitted to Journal of Belarusian State University: Physics.

2f. Cluster expansion for the description of condensed state: crystalline cell approach

A method for modifying the cluster virial expansion, which makes it possible to describe condensed state, is proposed. The method is based on replacing the averaging over the states of an ideal gas by the averaging over the states of an ideal crystal. The approach outlined differs from the well-known perturbation theory in that the basis with respect to which the expansion is performed is not a part of the original Hamiltonian but is introduced independently. The basis distribution conveys the main features of the solid state of matter, where the motion of molecules is of an oscillatory nature with respect to the lattice sites. As a result, the Hamiltonian of the basic reference system is represented by the sum of single-particle cell mean force potentials. It is shown how the Mayer functions can be modified so that they would act as a small parameter for the subsequent expansion of the thermodynamic potential by cumulant expansions. From the condition of independence of the initial partition function from the introduced potentials of the mean forces, a system of integral equations determining the above potentials is obtained. The expression for the free energy functional is obtained with the two first terms of its expansion in correlations taken into account. It is shown that the obtained equations satisfy several optimization

conditions for the parameters characterizing the properties of the reference system and the initial system. The thermodynamic consistency of various methods for calculating the thermodynamic characteristics of a condensed medium both in the canonical and in the grand canonical ensembles is proved. A possibility of using the developed approach to take into account not only short-range but also long-range interactions is shown.

The work was started during the secondments of the BSTU employee, Dr. George Bokun (to ICMP) and prolonged during the secondment of the ICMP employee Prof. Myroslav Holovko (to BSTU). The results are published in Ref. [16]

2g. Monte Carlo simulation of diffusion and electric conductivity in Coulomb systems

A specific feature of diffusion in one-dimensional channels is that, in view of the small lumen of the channel, particles cannot outrun each other and the sequence of their location along the channel is maintained throughout their movement. This leads to the fact that the average square of the displacement of individual particles is proportional to the square root of time, that is, the subdiffusion regime is realized. The effect of long-range Coulomb interaction on subdiffusion characteristics and electrical conductivity of one-dimensional systems is of interest.

The results of modeling the motion of particles with Coulomb interaction in 1d system are shown in Fig. 20. It was assumed that the particles move along the potential relief with minima at the lattice sites with the potential depths E_g.

The mean square displacement of the center of mass of the particles, through which the kinetic diffusion coefficient and electrical conductivity of the system is expressed, demonstrates the classical diffusion behavior and increases in proportion to time, while the mean square displacement of individual particles increases in proportion to the square root of time

$$\left\langle (\Delta x_{\mathrm{CM}})^2 \right\rangle = 2Dt, \qquad \left\langle (\Delta x)^2 \right\rangle = 2D_{1/2}t^{1/2},$$

as the depths of the potential wells E_g increase, the mean squares of the displacements decrease in proportion to $\exp(-\beta E_g)$.

The dependence of the electrical conductivity of the system on temperature was found to be of Arrhenius type. The activation energy was found to be equal to 0.047 eV when

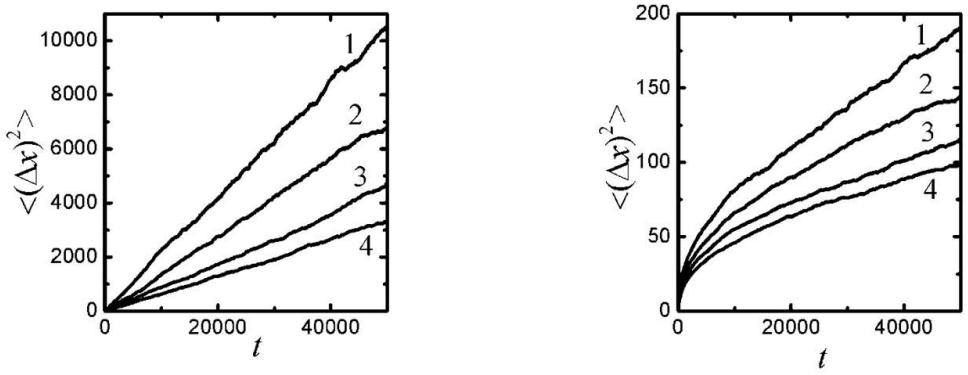

FIG. 20: The dependence of the mean square displacement of particles with the Coulomb interparticle interaction on time (in Monte Carlo steps). The left panel is for the center of mass, the right panel is for individual particles. The lattice concentration of particles is 1/12, the dielectric constant 40, the temperature 300 K, the lattice parameter 0.4 nm. The depths of the potential wells E_g in electron volts: 0.04 (1), 0.5 (2), 0.06 (3), 0.07 (4).

the potential wells E_g were equal to 0.05 eV. This means that Coulomb interactions in 1d-systems weakly influence the electrical conductivity.

A three-dimensional model of oxide ceramics containing a grain and an intergranular boundary is considered. The boundary is described by layers characterized by additional intersite energy barriers. Ewald's summation was incorporated to determine the Coulomb energy. The simulations of the described system using the kinetic Monte-Carlo method were started.

The work was performed during the secondments of the BSTU employees, Prof. Vyacheslav Vikhrenko and Dr. Ruslan Lasovsky (to CSIC), and the ICMP employee Dr. Taras Patsahan (to BSTU). The results are presented at the conferences and submitted for the publication. The work is in progress and the collaboration will continue.

DISSEMINATION AND PUBLICATION ACTIVITIES

Activity 1.

Y. V. Kalyuzhnyi; M. Holovko; J. Reščič; P. T. Cummings, *Primitive models of room temperature ionic liquids. Liquid-gas phase coexistence*, J. Mol. Liq. **270**, 7-13 (2018).

Activity 2.

O.V. Patsahan, T.M. Patsahan, M.F. Holovko, *Vapor-liquid phase behavior of a size-asymmetric model of ionic fluids confined in a disordered matrix: The collective-variables-based approach*, Phys. Rev. E **97**, 022109 (2018).

Activity 3.

O.V. Patsahan, T.M. Patsahan, M.F. Holovko, *Vapour-liquid critical parameters of a 2:1 primitive model of ionic fluids confined in disordered porous media*, J. Mol. Liq. **270**, 97-105 (2018).

Activity 4.

O.V. Patsahan, T.M. Patsahan, *Phase behaviour in ionic solutions: restricted primitive model of ionic liquid in explicit neutral solvent*, Preprint arxiv:1809.08043, http://arxiv.org/abs/1809.08043; J. Mol. Liq. (accepted), https://doi.org/10.1016/j.molliq.2018.11.078.

Activity 5.

M. Hvozd, T. Patsahan, M. Holovko, *Isotropic-nematic transition and demixing behaviour in binary mixtures of hard spheres and hard spherocylinders confined in a disordered porous medium: Scaled particle theory*, J. Phys. Chem. B **122**, 5534-5546 (2018).

Activity 6.

K. Breitsprecher, C. Holm, S. Kondrat, *Charge Me Slowly, I Am in a Hurry: Optimizing Charge–Discharge Cycles in Nanoporous Supercapacitors*, ACS Nano **12** (10), 9733-9741 (2018).

Activity 7.

A.Ciach, *Simple theory for oscillatory charge profile in ionic liquids near a charged wall*, publication, J. Mol. Liq. **270**, 138 (2018)

Activity 8.

C. Cruz, A. Ciach, E. Lomba and S Kondrat, *Electrical Double Layers Close to Ionic Liquid-Solvent Demixing*, publication, submitted.

Activity 9.

A. Ciach, "Simple theory for oscillatory charge profile in ionic liquids near a charged wall" poster, Tenth Liblice Conference on the Statistical Mechanics of Liquids, June 17-22, 2018 Srni (Sumava National Park), Czech Republic.

Activity 10.

G. Bokun, D. di Caprio, My. Holovko, V. Vikhrenko, *The system of mobile ions in lattice models: Screening effects, thermodynamic and electrophysical properties*, J. Mol. Liq. **270** (2018) 183-190.

Activity 11.

T. Patsahan, G. Bokun, D. di Caprio, M. Holovko, and V. Vikhrenko, *The effect of short-range interaction and correlation on the charge and electric field distribution in a model solid electrolyte*, Solid State Ionics (submitted).

Activity 12.

T. Patsahan, G. Bokun, D. di Caprio, M. Holovko, V. Vikhrenko, "The effect of electric field on the charge distribution and electric potential in a model solid electrolyte", Poster presentation at 13th International Symposium on Systems with Fast Ionic Transport. 3–7 July 2018, Minsk, Book of Abstracts, P. 61.

Activity 13.

G.S. Bokun, D. di Caprio, *Charge and concentration distribution of charge carriers in solid*

electrolyte between flat electrodes, Journal of Belarusian State University: Physics. (In press, in Russian).

Activity 14.

G.S. Bokun, M.F. Holovko, *Cluster expansion for the description of condensed state: crystalline cell approach*, Condens. Matter Phys. **21** (2018) 43501.

Activity 15.

R.N. Lasovsky, V.S. Vikhrenko, T. Patsahan, D. Gapanjuk, "Influence of a grain boundary on electric current and charge distribution: 3D Monte Carlo simulation of a lattice model", Poster presentation at 13th International Symposium on Systems with Fast Ionic Transport (ISSFIT-13), 3–7 July 2018, Minsk, P. 62.

Activity 16.

R.N. Lasovsky, V.S. Vikhrenko, "Computer simulation of three-dimensional systems with Coulomb interaction", oral presentation at the conference "Fullerenes and nanostructutes in condensed media", 20–23 August 2018, Minsk, p. 79–82.

Activity 17.

R.N. Lasovsky, Y.G. Groda, V.S. Vikhrenko, "Diffusion and electrical conductivity in one-dimensional lattice systems", oral presentation at the conference "Solid State Physics-2018. Modern problems of solid state physics", 25–28 September 2018, Minsk, Vol. 3, p. 34–36 (2018).

Activity 18.

M. Holovko, T. Patsahan, M. Hvozd, "Isotropic-nematic transition and demixing behaviour in binary mixtures of hard spheres and hard spherocylinders confined in disordered porous medium", oral presentation at 8th International Conference Physics of Liquid Matter: Mod-

ern Problems, Kyiv (Ukraine), 18-22.05.2018.

---

[1] M.F. Holovko, Y.V. Kalyuzhnyi, *Mol.Phys.* **73** 1145 (1991).

[2] L. Blum, J.S. Hoye, *J. Phys. Chem.* **81** 1311 (1977).

[3] A.Z. Panagiotopoulos, *J.Chem.Phys.* **116** 3007 (2002).

[4] L.P.N. Rebelo, J.N.C. Lopes, E. Filipe, *J.Phys.Chem.B* **109** 6040 (2005).

[5] Y. V. Kalyuzhnyi, M. Holovko, J. Reščič, P. T. Cummings, *J. Mol. Phys.* **270**, 7-13 (2018).

[6] O.V. Patsahan, T.M. Patsahan, preprint arXiv:1809.08043, http://arxiv.org/abs/1809.08043; J. Mol. Phys. (accepted), https://doi.org/10.1016/j.molliq.2018.11.078.

[7] T. Kristóf, D. Boda, I. Szalai, D. Henderson, *J. Chem. Phys.* **113** 7488-7491 (2000) .

[8] P.U. Kenkare, C.K. Hall, C. Caccamo, *J. Chem. Phys.* **103** 8098-8110 (1995).

[9] H.R. Dittmar, W.H. Schröer, *J. Phys.Chem. B* **113** 1249-1252 (2009).

[10] M. Holovko, T. Patsahan, M. Hvozd, "Isotropic-nematic transition and demixing behaviour in binary mixtures of hard spheres and hard spherocylinders confined in disordered porous medium", 8th International Conference Physics of Liquid Matter: Modern Problems, Kyiv (Ukraine), 18-22.05.2018, Book of abstracts, 11-10O (2018).

[11] M. Hvozd, T. Patsahan, M. Holovko, *J. Phys. Chem. B* **122** 5534–5546 (2018).

[12] O.V. Patsahan, T.M. Patsahan, M.F. Holovko, *Phys. Rev. E* **97**, 022109 (2018).

[13] O.V. Patsahan, T.M. Patsahan, M.F. Holovko, *J. Mol. Liq.* **270**, 97-105 (2018).

[14] K Breitsprecher, C Holm, S Kondrat, *ACS Nano* **12** 9733-9741 (2018).

[15] G. Bokun, D. di Caprio, M. Holovko, V. Vikhrenko, *J. Mol. Liq.* **270** 183-190 (2018).

[16] G.S. Bokun, M.F. Holovko, *Condens. Matter Phys.* **21** 43501 (2018).